Self-Assembling Peptide Nanotubes

Jeffrey D. Hartgerink, Juan R. Granja,† Ronald A. Milligan, and M. Reza Ghadiri*

Contribution from the Departments of Chemistry, Molecular Biology, and Cell Biology, The Scripps Research Institute, La Jolla, California 92037

Received September 6, 1995[⊗]

Abstract: The general design criteria and synthesis of four new peptide-based solid-state tubular array structures are described. Peptide nanotubes, which are extended tubular β-sheet-like structures, are constructed by the self-assembly of flat, ring-shaped peptide subunits made up of alternating D- and L-amino acid residues. Peptide self-assembly is directed by the formation of an extensive network of intersubunit hydrogen bonds. In the crystal structures, nanotubes are stabilized by intertubular hydrophobic packing interactions. Peptide nanotubes exhibit good mechanical and thermal stabilities in water and are stable for long periods of times in most common organic solvents including DMF and DMSO. The remarkable stability of peptide nanotubes can be attributed to the highly cooperative nature of the noncovalent interactions throughout the crystal lattice. Nanotube structures were characterized by cryoelectron microscopy, electron diffraction, Fourier-transform infrared spectroscopy, and crystal structure modeling. This study also serves to exemplify the predictive structural aspects of the peptide self-assembly process.

Introduction

Recently, we reported the design and construction of open-ended hollow tubular objects based on the self-assembly of flat, ring-shaped cyclic peptide subunits.[1] These artificial tubular constructs constitute a new class of synthetically readily accessible peptide-based biomaterials having unique structural and functional properties. Peptide nanotubes are constructed by highly convergent noncovalent processes by which cyclic peptides rapidly self-assemble and organize into ultralarge well-ordered three-dimensional structures, upon an appropriate chemical- or medium-induced triggering. The properties of the outer surface and the internal diameter of peptide nanotubes can be adjusted simply by the choice of the amino acid side chain functionalities and the ring size of the peptide subunit employed.[1−3] This design flexibility, which is unique to this class of tubular structures, has already enabled application of peptide nanotubes to the design of biologically-relevant transmembrane ion channels and pore structures.[2] Here, we detail the general design criteria for the construction of such ensembles and describe the synthesis and characterization of four new members of this family of structures. This study serves to exemplify the predictive structural aspects of the peptide self-assembly process.

Design Principles

Peptide- and protein-based tubular structures are well precedented in Nature. Tobacco mosaic virus, bacterial pili, and microtubulines are but a few remarkable examples of natural tubular assemblies. Moreover, the antibiotic gramicidin A, is a transmembrane ion-channel-forming linear polypeptide made up of alternating D- and L-amino acids which folds in lipid membranes into tubular β-helixes.[4] Synthetic poly(D,L-γ-benzylglutamyl) peptides have also been shown to adopt gramicidin-like β-helix structures.[5] Relevant to our work on peptide nanotubes, De Santis *et al*. within the context of a theoretical conformational analysis of linear poly-D,L-peptides had suggested in 1974 the possibility of forming cylindrical structures from cyclic peptides.[6] However, early attempts at the design of peptide tubular ensembles based on those principles were unsuccessful as evidenced by X-ray crystal structure analysis.[7a,b]

According to our design principles,[1] cyclic peptide structures made up of an even number of alternating D- and L-amino acid residues, tend to minimize nonbonded intramolecular transannular side chain−side chain and side chain−backbone interactions by adopting (or sampling) a flat ring-shaped conformation in which all backbone amide functionalities lie approximately perpendicular to the plane of the ring structure. Furthermore, because of the local conformational and steric constraints imposed by the alternating amino acid backbone configuration, all amino acid side chains point outward away from the center of the peptide ring structure, thus leaving it free to form a tubular core structure. In this conformation, the peptide subunits can stack to furnish contiguously hydrogen-bonded β-sheet-like tubular ensembles (Figure 1). Among the factors which directly affect the peptide self-assembly process, ring size of the peptide subunit, preference for a particular ring stacking arrangement, relative sheet register, and identity of the amino acid side chains employed exert the most critical influence.

Influence of the Cyclic Peptide Ring Size. Ring strain and conformational stability are the two most important factors in the peptide self-assembly process influenced by the size of the cyclic peptide employed. Cyclic D,L-peptides of less than six residues have too small of an internal diameter and may have

† Present address: Department of Organic Chemistry, Universidade de Santiago de Compostelo, Spain.

⊗ Abstract published in *Advance ACS Abstracts,* December 1, 1995.

(1) (a) Ghadiri, M. R.; Granja, J. R.; Milligan, R. A.; McRee, D. E.; Khazanovich, N. *Nature* **1993**, *366*, 324−327. (b) Khazanovich, N.; Granja, J. R.; McRee, D. E.; Milligan, R. A.; Ghadiri, M. R. *J. Am. Chem. Soc.* **1994**, *116*, 6011−6012. (c) Ghadiri, M. R. *Adv. Mater.* **1995**, *7*, 675−677.

(2) (a) Ghadiri, M. R.; Granja, J. R.; Buehler, L. *Nature* **1994**, *369*, 301−304. (b) Granja, J. R.; Ghadiri, M. R. *J. Am. Chem. Soc.* **1994**, *116*, 10785−10786.

(3) (a) Ghadiri, M. R.; Kobayashi, K.; Granja, J. R.; Chadha, R. K.; McRee, D. E. *Angew. Chem., Int. Ed. Engl.* **1995**, *34*, 93−95. (b) Kobayashi, K.; Granja, J. R.; Ghadiri, M. R. *Ibid.* **1995**, *34*, 95−98.

(4) Ketchem, R. R.; Hu, W.; Cross, T. A. *Science* **1993**, *261*, 1457−1460.

(5) Lotz, B.; Colonna-Cesari, F.; Heitz, F.; Spach, G. *J. Mol. Biol.* **1976**, *106*, 915−942.

(6) De Santis, P.; Morosetti, S.; Rizzo, R. *Macromolecules* **1974**, *7*, 52−58.

(7) (a) Tomasic, L.; Lorenzi, G. P. *Helv. Chim. Acta* **1978**, *70*, 1012−1016. (b) Pavone, V.; Benedetti, E.; Di Blasio, B.; Lombardi, A.; Pedone, C.; Tomasich, L.; Lorenzi, G. P. *Biopolymers* **1989**, *28*, 215−223. (c) Sun, X.; Lorenzi, G. P. *Helv. Chim. Acta* **1994**, *77*, 1520−1526.

0002-7863/96/1518-0043$12.00/0

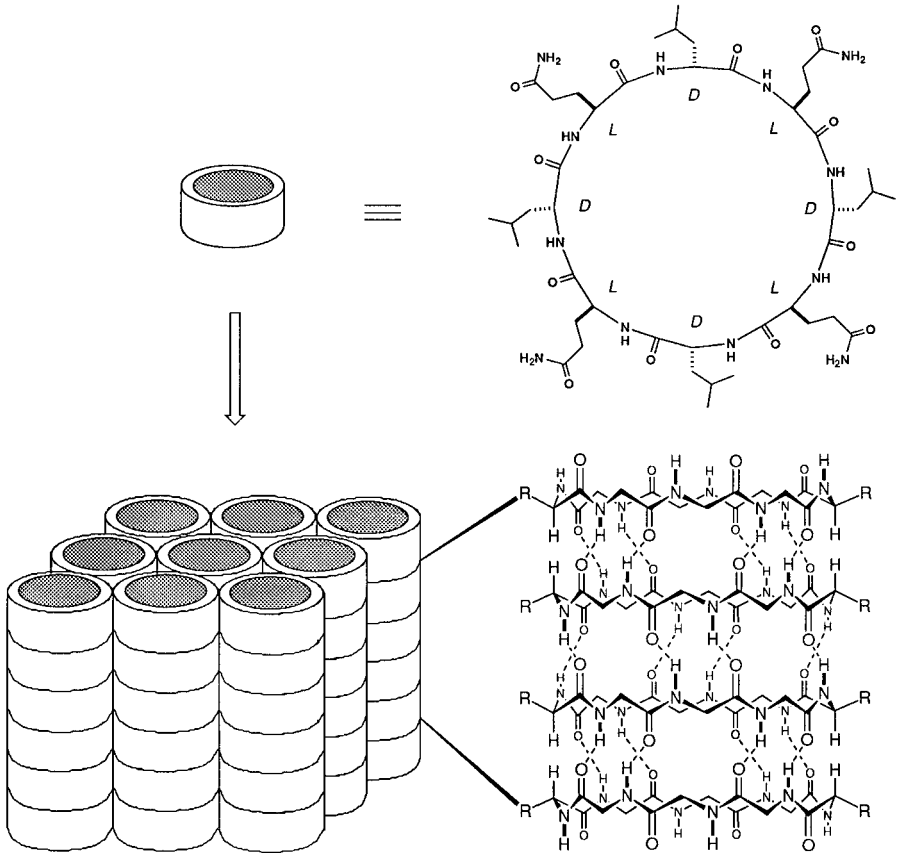

Figure 1. Cyclic peptide structures with alternating D- and L-amino acids adopting flat ring-shaped conformations and, depending on the peptide sequence and the conditions employed, assembling into ordered parallel arrays of solid-state nanotubes. The illustration emphasizes the antiparallel ring stacking and the presence of extensive intersubunit hydrogen-bonding interactions (for clarity most side chains are omitted).

prohibitively large ring strain to allow the peptide backbone to adopt the required geometry for stacking and intermolecular hydrogen-bonding interactions and thus are not useful in the context of nanotube designs. Conversely, too large of a ring structure, due to the greater flexibility of the peptide backbone, may not sample in the flat ring-shaped conformational state to effectively take part in the nanotube self-assembly process. Molecular modeling and experimental studies have indicated that eight-residue cyclic peptides possess the optimum balance of a low-strain ring structure and the desired flat ring-shaped conformational stability. For example, recent studies have shown that, while the eight-residue cyclic peptide cyclo[-(D-^{Me}NAla-L-Phe)$_4$-] can self-assemble into the expected hydrogen-bonded cylindrical ensemble both in nonpolar organic solvents (2D ^{1}H NMR studies) as well as in the solid state (high-resolution X-ray crystallographic analysis),[3] the smaller cyclic hexapeptide counterpart cyclo[-(D-^{Me}NAla-L-Phe)$_3$-] cannot.[8] We have attributed this observation to the high energy required for the amide backbone to adopt the necessary conformation for cooperative ring-stacking interactions. However, contrary to our results, a recent study using a related peptide structure has reported formation of a dimeric hydrogen-bonded cylindrical structure from the hexameric peptide subunit cyclo[-(D-Leu-L-^{Me}NLeu)$_3$-].[7c] Yet, previous studies from the same laboratory had indicated that cyclic hexapeptides cyclo[-(L-Val-D-Val)$_3$-] and cyclo[-(L-Phe-D-Phe)$_3$-] do not form tubular ensembles in the solid state as evidenced by single-crystal X-ray structural analysis.[7b] Together, the above studies seem to indicate that the formation of nanotube structures from the more strained six-residue cyclic peptides may not be a general phenomenon and may be highly dependent on the peptide sequence, the solvent, and the crystallization conditions employed.

Recent studies from our laboratory have documented the formation of tubular solid-state arrays and/or transmembrane channels and pore structures made from eight-,[1a,2a,3] ten-,[2b] and twelve-residue[1b] cyclic peptide subunits which give tubular ensembles with internal van der Waals pore diameters of 7, 10, and 13 Å, respectively. Whether peptide nanotubes can be assembled from larger cyclic peptide subunits is the topic of future investigations. In the present study, in order to better probe the influence of directed noncovalent interactions in the self-assembly of solid-state tubular arrays, we have limited our designs to eight-residue cyclic peptide subunits.

Ring Stacking Arrangements. The backbone−backbone intermolecular hydrogen-bonding interactions can proceed, in principle, via either parallel or antiparallel β-sheet-like ring-stacking arrangements (Figure 2). However, molecular modeling and a number of experimental observations[1−3] suggest a marked preference for the antiparallel arrangement. Formation of the antiparallel ring-stacked arrangement in self-assembled nanotubes has been supported by the symmetries observed in the electron diffraction patterns and the position of the amide I bands in the FT-IR spectra. Furthermore, recent solution-phase ^{1}H NMR studies and high-resolution X-ray crystallographic analyses of a structurally related but simpler member of this family have unequivocally indicated the preference for the antiparallel arrangement.[3] Therefore, in solution or in the solid-state—in the absence of an unusually strong crystal packing interactions—formation of the extended antiparallel β-sheet-like hydrogen-bonded tubular structure is expected to be the more favored arrangement.

(8) Kobayashi, K.; Ghadiri, M. R. Unpublished results.

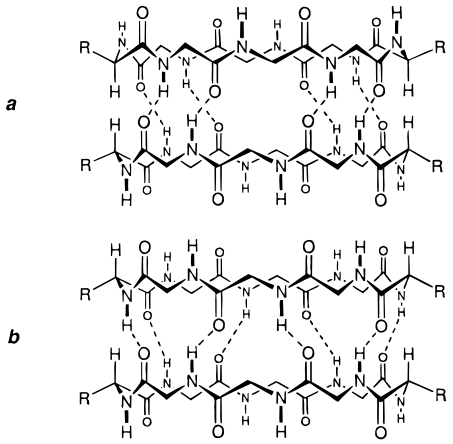

Figure 2. Peptide self-assembly producing antiparallel (a) and parallel (b) stacking arrangements.

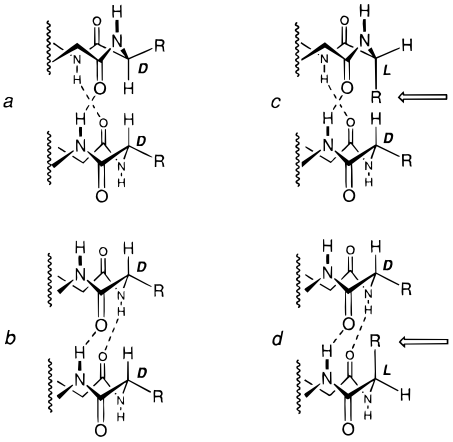

Figure 3. Homochiral residues forming cross-strand near-neighbor residues in either the antiparallel (a) or parallel (b) β-sheet arrangements. Alternative heterochiral cross-strand arrangements have prohibitively large intersubunit side chain−backbone steric interactions (arrows), in both antiparallel (c) and parallel (d) orientations, to allow ring stacking and intersubunit backbone−backbone hydrogen-bonding interactions. For clarity, only the right edges of the hydrogen-bonded stacked subunits (Figure 2) are shown.

Relative Sheet Register. The strategy employed in the design of self-assembling peptide nanotubes satisfies two essential criteria for directing the formation of β-sheet ensembles. It provides control over the subunit facial selectivity, by favoring the antiparallel ring stacking arrangement, and the means for rigorously regulating the relative sheet register, thereby setting the identities of the cross-strand nearest neighbor residues. Control over the sheet register is due to the alternating D- and L-backbone chirality which constrains the β-sheet structure such that only *homochiral* residues can make up the cross-strand β-sheet nearest pairs. This restriction is the direct consequence of the intermolecular hydrogen-bonding interaction dictated by the juxtaposition of backbone amide hydrogen bond donor and acceptor sites, as well as the large side chain−backbone steric interactions present in alternative sheet registers and side chain arrangements (Figure 3). Nevertheless, despite this high degree of structural control, for an even-numbered n-residue cyclic D- and L-peptide structure in a two-stranded antiparallel β-sheet-like ensemble, there are a maximum of $n/2$ possible relative ring registers.[3b] The isomeric diversity can be reduced to a unique structure simply by employing $C_{n/2}$ symmetrical (perpendicular to the ring structure) peptide subunits. As indicated below, symmetry considerations in the design of peptide subunits are also indispensable for engineering three-dimensional crystalline tubular ensembles.

Sequence Selection and Design of Three-Dimensional Nanotube Crystal Structures. Detailed structural assignment is often the most critical issue in studying supramolecular systems. This inherent difficulty is often the primary obstacle preventing rigorous assessment of the efficacy of the underlying design principles and further generation of new and improved systems with desired structural and functional properties. There are only a handful of spectroscopic techniques, such as NMR spectroscopy, electron diffraction analysis, and X-ray crystallography, which can provide detailed three-dimensional structural information on large-molecule systems. Among these techniques, the latter two are most suitable for the large self-assembled tubular objects studied here and both necessitate the availability of highly ordered crystalline specimens. Therefore, as an essential design feature, we focused on the design of three-dimensional nanotube crystals.

Design of predetermined three-dimensional crystals is often a difficult task because of the large number of factors which can influence the crystallization process and the inter- and intramolecular noncovalent interactions in the solid state. We hypothesized that the subunit self-assembly, which is most favored along the tube axis, due to the formation of highly oriented backbone−backbone hydrogen-bonding network, should ensure crystalline order in that dimension (along the crystallographic *a* axis). In order to favor crystal packing and growth in the other two dimensions (along the crystallographic *b* and *c* axes), we made the following conceptual design simplification. Similar to simple helical folding motifs found in natural proteins, we investigated the possibility of forming an ordered parallel packed array of nanotube solid-state structures. If conceptually single nanotubes are viewed as a novel form of protein secondary structure (β-tubes), then the three-dimensional crystal-packing issue is equivalent to the rational design of side chain−side chain noncovalent intertubular interactions. Natural proteins exploit hydrogen-bonding, electrostatic, van der Waals, and hydrophobic interactions in directing three-dimensional folding arrangements. Among these, entropically driven hydrophobic interactions provide the most effective driving force in aqueous solution and have been previously exploited in a number of artificial protein designs.[9] In the present design we chose to evaluate the effectiveness of side chain−side chain hydrophobic and hydrogen-bonding interactions in nanotube crystal engineering experiments. We hypothesized that the intertubular hydrophobic interactions would have the most dominant effect in orienting nanotubes in the solid state. Therefore, in the four nanotube constructs designed for the present study, we chose to study the effects of increasing hydrophobic surface contact by employing alanine, valine, leucine, and phenylalanine as the nonpolar amino acid residues in the design of the peptide subunits. Furthermore, in order to keep the number of variables to a minimum, we employed glutamine as the only polar amino acid residue. The choice of Gln was based on the unique hydrogen-bonding donor/acceptor capability of its amide side chain and because it can, in principle, participate in both intra- and intertubular hydrogen-bonding interactions which were thought to provide additional structural stability and order to the system (Figure 4). Peptide constructs were designed to be C_4 symmetric in order to produce a single nanotube isomer. The subunit's symmetry and the expected

(9) (a) Ghadiri, M. R.; Case, M. A. *Angew. Chem., Int. Ed. Engl.* **1993**, *32*, 1594−1597. (b) M. Mutter; S. Vuilleumier *Angew. Chem., Int. Ed. Engl.* **1989**, *28*, 535. (c) Betz, S. F.; Raleigh, D. P.; DeGRado, W. F. *Curr. Opin. Struct. Biol.* **1993**, *3*, 601. (d) Harbury, P. B.; Zhang, T.; Kim, P. S.; Alber, T. *Science* **1993**, *262*, 1401.

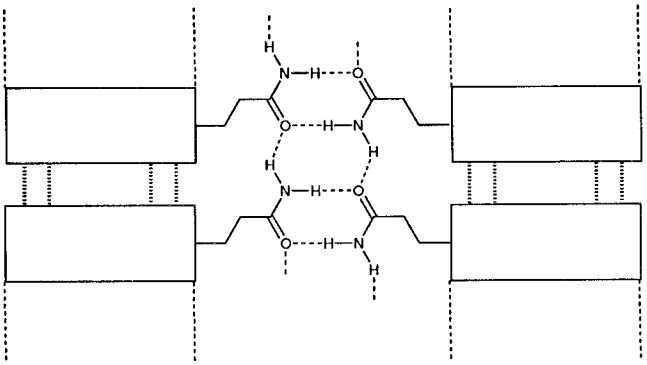

Figure 4. Glutamine side chains participating in both intra- and intertube hydrogen-bonding interactions, is thought to add further stability and long-range order to the solid-state tubular array systems. The figure illustrates the maximally hydrogen bonded structure (peptide subunits are represented by rectangular blocks).

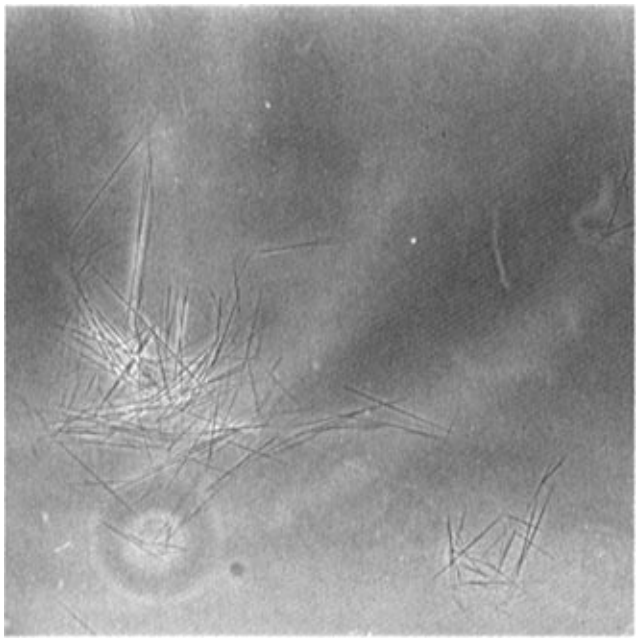

Figure 5. Optical micrograph of c-[(Gln-D-Ala)$_4$-] nanotube crystals. Nanotube crystals from the other three peptide subunits show similar images.

hydrogen-bond-directed arrangement of the peptide subunits was expected to favor formation of tetragonal crystal space groups (*P*,*I*).

Results

All four cyclic peptides assemble under appropriate conditions to form needle-shaped microcrystals as large as 200 × 10 μm (Figure 5). Low-dose cryoelectron microscopy,[10] Fourier transform infrared spectroscopy (FT-IR), electron diffraction, and molecular modeling were used to characterize and assign the structural features of nanotube crystals. Cryoelectron microscopy at high magnifications revealed characteristic striations running along the long axis of the crystals. These striations were spaced at a distance that corresponds to the van der Waals width of a single flat ring-shaped cyclic peptide and represent images of individual nanotubes packed side by side in parallel (Figure 6).

Nanotube crystal arrays formed by the self-assembly of the peptide subunits display FT-IR spectra in the amide I and amide

(10) Milligan, R. A.; Flicker, P. F. *J. Cell. Biol.* **1987**, *105*, 29−39.

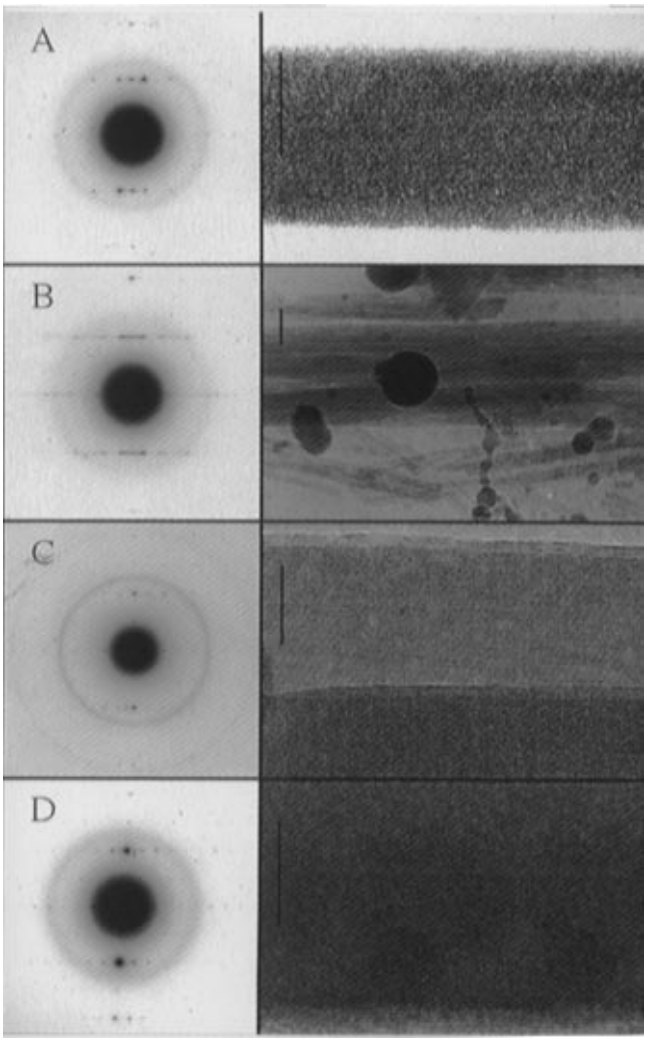

Figure 6. Electron diffraction (left panels) and low-dose cryoelectron micrographs (right panels) of frozen hydrated nanotube crystals (scale bars, 50 nm): (A) c-[(Gln-D-Ala)$_4$-], (B) c-[(Gln-D-Val)$_4$-], (C) c-[(Gln-D-Leu)$_4$-], (D) c-[(Gln-D-Phe)$_4$-].

Table 1. FT-IR Data (cm^{-1})

nanotubes	amide Ia	amide Ib	amide II	N−H stretch	intersubunit distance (Å)
c-[(Gln-D-Ala)$_4$-]	1630	1672	1549	3282	4.74 (4.80)
c-[(Gln-D-Val)$_4$-]	1630	1687	1542	3292	4.77 (4.85)
c-[(Gln-D-Leu)$_4$-]	1629	1688	1540	3278	4.72 (4.75)
c-[(Gln-D-Phe)$_4$-]	1629	1678	1541	3280	4.73 (4.83)

II regions that are characteristic of extensively hydrogen-bonded β-sheet-like networks[11] (Table 1, Figure 7). Moreover, the N−H stretching frequency occurring between 3278 and 3292 cm^{-1} also correspond to a tightly hydrogen bonded ring-stacked network with an average intersubunit distance of 4.7−4.8 Å. The interpeptide distances above obtained from the Krimm's analysis[11b] of the N−H stretching frequencies correlate reasonably well with the numbers obtained independently from electron diffraction data (*vide infra*).

Nanotube crystal structures were modeled on the basis of the analysis of cryoelectron diffraction patterns. Because of the symmetry of the peptide subunits employed, electron diffraction patterns can provide the unit cell size and angles. Using the above data, models of the nanotubes were constructed and

(11) (a) Haris, P. I.; Chapman, D. *Biopolymers (Peptide Sci.)* **1995**, *37*, 251−263. (b) Krimm, S.; Bandekar, J. In *Advances in Protein Chemistry*; Anfinsen, C. B.; Edsall, J. T., Richards, F. M., Eds.; Academic Press: Orlando, FL, 1986; pp 181−364.

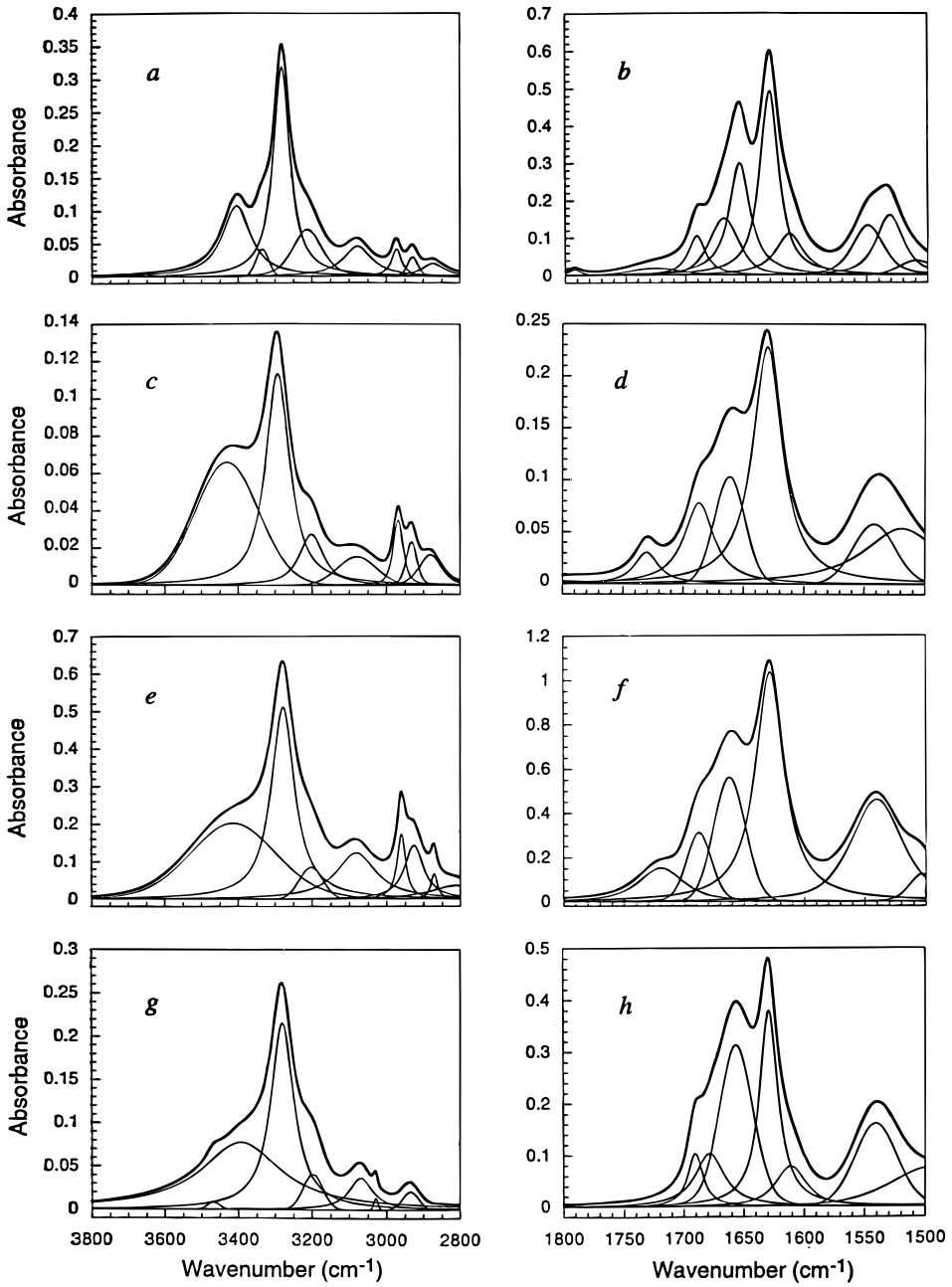

Figure 7. Infrared spectra (at 4-cm^{-1} resolution, KBr pellet) of N−H stretch (a, c, e, and g) and amide I and amide II regions (b, d, f, and h) of nanotube crystals (from top to bottom): c-[(Gln-D-Ala)$_4$-], c-[(Gln-D-Val)$_4$-], c-[(Gln-D-Leu)$_4$-], and c-[(Gln-D-Phe)$_4$-].

Table 2. Unit Cell Parameters and Nanotube Crystal Lengths Derived from the Analyses of Electron Diffraction Patterns, Low-Dose Cryo-EM Imaging, and Optical Microscopy

	unit cell dimens and angles						striation	av bundle
nanotubes	*a*	*b*	*c*	α	*β*	*γ*	spacing (Å)	length (μm)
c-[(Gln-D-Ala)$_4$-]	9.60	21.2	21.2	90	90	90	15	60−100
c-[(Gln-D-Val)$_4$-]	9.7	16.1 ± 1.0		ND	ND	ND	ND	80−120
c-[(Gln-D-Leu)$_4$-]	9.50	18.30	18.30	90	90	90	18.3	100−200
c-[(Gln-D-Phe)$_4$-]	9.66	18.44	18.44	90	94	94	18.5	10−20

structure factors were calculated which compared favorably with the actual diffraction patterns and intensities. In addition, each crystal model was examined by Procheck[12] to reveal and eliminate any bad crystal contacts.

Highly ordered nanotube crystals were obtained from peptide subunits c-[(Gln-D-Ala)$_4$-], c-[(Gln-D-Leu)$_4$-], and c-[(Gln-D-Phe)$_4$-]. Cryoelectron diffraction patterns which often extended to 1.2 Å resolution were indicative of highly ordered specimens and were used to obtain the unit cell dimensions and angles (Table 2). Low-dose cryo transmission electron micrographs each showed longitudinal striations due to the parallel crystal packing of individual nanotubes. On the other hand, the peptide subunit c-[(Gln-D-Val)$_4$-] only formed semicrystalline needles which did not show the characteristic striations in the TEM images. However, from image analysis, these nanotubes seemed to be made up of an aggregation of many thousands of smaller

(12) Laskowski, R. A.; MacArthur, M. W.; Moss, D. S.; Thornton, J. M. *J. Appl. Crystallogr.* **1993**, *26*, 283−291.

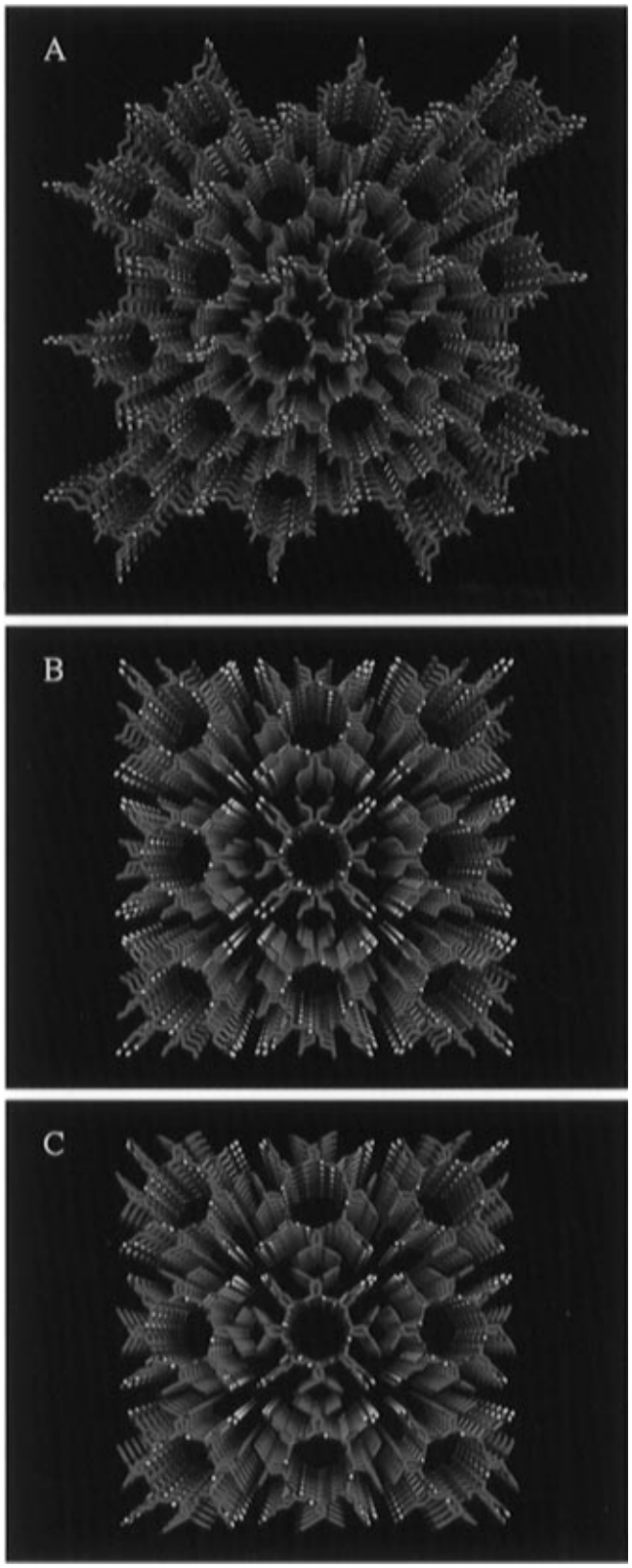

Figure 8. Models of the calculated three-dimensional nanotube crystal structures viewed along the *a* axes: (a) [(Gln-D-Ala)$_4$-], (b) c-[(Gln-D-Leu)$_4$-], and (c) c-[(Gln-D-Phe)$_4$-]. Models are scaled to allow direct visual comparison.

(about 10 nm long) nanotubes all generally arranged in the same orientation. Electron diffraction images support this interpretation, showing strong structure factors corresponding to the stacking of cyclic peptides but a blurring along the *b* and *c* axes implying that the lateral packing is not well ordered. Models of the calculated crystal structures are shown in Figure 8.

Discussion

Peptide subunits were synthesized on solid support and characterized by ^{1}H NMR spectroscopy and mass spectrometry. Subunits assemble in high yields in aqueous TFA mixtures to form needle-shaped crystalline objects. Nanotube crystals do not appear to form lattice inclusions with TFA as judged by their remarkable stabilities in alkaline solutions. Furthermore, only traces of TFA could be detected by FT-IR spectroscopy, which may be attributed to the small amounts remaining inside the water-filled pores of the nanotube crystals. Nanotube crystals exhibit good mechanical stabilities and can withstand repeated centrifugation ($<$15000*g*) and strong vortex mixing. Crystals also seem to be stable when dehydrated in vacuum as judged by transmission electron and optical microscopy of rehydrated samples. Nanotube crystals are stable to highly acidic (pH = 1) and strongly basic solutions (pH = 14) and can survive even boiling water. They also exhibit remarkable long-term stability in most common polar and nonpolar organic solvents including hexafluoroisopropyl alcohol, DMF, and DMSO with the exception of nanotubes made from c-[(Gln-D-Leu)$_4$-] which dissolve in neat DMSO and hexafluoroisopropyl alcohol.

The remarkable stability of peptide nanotubes can be attributed to the highly cooperative nature of the self-assembled structure which simultaneously reinforces multiple noncovalent interactions throughout the lattice. Enthalpically driven hydrogen-bonding networks are reinforced with entropically driven hydrophobic interactions such that, in aqueous solutions, water cannot compete with backbone−backbone hydrogen bonding to displace peptide subunits from the self-assembled structure. In addition, low solubility of peptide subunits even in highly polar organic solvents prevents dissociation and breakup of hydrophobic interactions which maintain intertubular packing interactions. Furthermore, because hydrophobic and hydrogen-bonding interactions have opposing temperature-dependent energetic contributions in aqueous solutions, nanotubes are also stable from below freezing temperatures to boiling water. Stability of the nanotube ensembles in highly acidic and alkaline solutions can be attributed to the absence of ionizable amino acid side chain functionalities within the peptide subunit sequences employed. Only under extremely acidic conditions such as neat TFA where peptide backbone is protonated can nanotube crystals dissociate to give monomeric peptide subunits.

Optical and electron microscopies show exclusive formation of rod-shaped crystalline objects (Figure 5). Formation of rod-shaped crystals is an expected consequence of the faster rate of self-assembly or crystal growth along the tube axis where the extensive network of cooperative backbone−backbone inter-subunit hydrogen-bonding stacking interactions take place. When samples were examined by high-resolution low-dose cryoelectron microscopy, longitudinal striations demarcating boundaries of nanotubes were observed (Figure 6). Image analysis revealed striation spacing of approximately 15.0, 18.3, and 18.5 Å for crystals made from c-[(Gln-D-Ala)$_4$-], c[(Gln-D-Leu)$_4$-], and c-[(Gln-D-Phe)$_4$-] peptide subunits, respectively (nanotubes made from c-[(Gln-D-Val)$_4$-] did not show striations due to disordered aggregation of small nanotube ensembles). The increase in striation spacing mirrors the increase in van der Waals radii of the nonpolar side chains engaged in intertubular hydrophobic packing interactions.

FT-IR spectroscopy is a sensitive technique which can provide valuable structural information about the self-assembled nanotube structures and the mode of hydrogen-bonding interactions between the stacked peptide subunits.[11] The observed amide I bands at 1629−1630 cm^{-1} and amide II bands at 1540−1549

cm^{-1} are characteristic of β-sheet-like structures (Table 1). The position of N−H stretching frequency was used to gain valuable information regarding the geometry of the peptide subunits in the nanotube ensembles. Although N−H stretch is a highly localized mode, its frequency, normally seen between 3310 and 3270 cm^{-1}, depends on the strength of the N−H···O═C hydrogen bond and has been shown to be a sensitive reflection of structure and its variations. High-resolution structural data have been previously used by Krimm to correlate N−H stretching frequencies with the geometry of hydrogen bonds in several polypeptides.[11b] The basis data consist of hydrogen bonds which have HNO angles in the range of 3−10°, NHO angles in the range of about 165−175°, and hydrogen-bonding distances of 2.70−2.90 Å. The relationship permits the determination of the N···O distances from the observed N−H stretching frequency in the region of about 3200−3300 cm^{-1}. Therefore, the observed N−H stretching frequencies in the range of 3278−3292 cm^{-1} strongly support the presence of the tight network of hydrogen-bonded stacked subunits with an average intersubunit distance of 4.7−4.8 Å (Table 1). These values are in close agreement with the axial periodicities measured from the electron diffraction patterns (Table 2).

Analysis of the electron diffraction patterns have provided the most direct insight into the nanotube crystal structures and packing interactions. Electron diffraction patterns which extend to 1.2 Å resolution suggest the preponderance of a highly ordered crystalline specimen (patterns were recorded from single crystals laid flat on carbon grid supports with the incident electron beam normal to the long axis of the rod). Without exception, all four ensembles displayed highly ordered axial periodicities (along the tube axis *a*) in the range of 4.75−4.85 Å as expected from tightly hydrogen bonded peptide subunits stacked in an ideal antiparallel β-sheet-like arrangement. Diffraction patterns also showed meridional spacing of 21.2, 18.30, and 18.44 Å for crystals made from c-[(Gln-D-Ala)$_4$-], c-[(Gln-D-Leu)$_4$-], and c-[(Gln-D-Phe)$_4$-]. Meridional spots in the electron diffraction images of c-[(Gln-D-Val)$_4$-] were broad (16.1 ± 1.0 Å), suggesting not so well ordered lateral packing of nanotubes within the crystal lattice which also corroborate with the lack of observable longitudinal striations by low-dose cryo-TEM image analysis.

Analysis of the electron diffraction patterns were used to derive the unit cell parameters. Electron diffraction patterns only provide direct information about two of the three crystal axes: *a* and *b* or *c*. However, because of the symmetrical nature of the peptide subunits employed, *b* and *c* axes were expected to be identical in size. This expectation is borne out by a recent high-resolution X-ray crystal structure determination of two simpler but related tubular peptide ensembles as well as in the present case by the following experimental observations. Because of the thin rod shape of the crystals, they lay on the supporting carbon grid along the long axis (*a*) and either of the *ab* or *ac* faces. Therefore, electron diffraction patterns taken from a given sample must also reflect this statistical distribution. However, all diffraction patterns, taken from a given sample of crystals, show similar diffraction intensities and identical lattices. Therefore, *b* and *c* axes must indeed be identical in size—similar reasoning suggests that β and γ angles should also be equal. It must also be noted that the diffraction patterns did not show any symmetry other than the center of symmetry due to Friedel's law. The unit cell dimensions and angles which are given in Table 2 were used to build three-dimensional crystal structure models.

Ordinarily, building a crystal structure based only on the unit cell parameters is a difficult task because of the large number of possible conformational states of polypeptides. However, in the present case, several factors go hand in hand to limit the number of possibilities. From the observed axial spacing in the electron diffraction patterns, it is clearly evident that peptide subunits assume the expected flat ring conformation in the crystals. Furthermore, the only way to pack peptides to within a 4.7−4.8 Å distance is to have tightly hydrogen bonded backbone−backbone stacking interactions. Any significant deviation from the flat ring conformation prevents the peptide subunit from packing to within the observed distances due to prohibitively large side chain van der Waals contacts. Moreover, because of the relatively small size of the unit cells, only the flat conformer can fit within it. Therefore, modeling the peptide subunit within the box defined by the unit cell reduces to allowed rotations of the peptide within the *bc* plane. Several rotations were examined but only one fits based on the steric grounds. Furthermore, this orientation also places all hydrophobic side chains within van der Waals contact, thus producing extensive intertubular hydrophobic interactions in the crystal lattice. Peptide nanotube crystals all contain two peptide subunits per unit cell (one dimer) with the exception of c-[(Gln-D-Ala)$_4$-], where four peptide subunits (two dimers) occupy the unit cell—this crystal structure is nearly identical to the previously described crystal structure of the related peptide nanotube c-[(Gln-D-Ala-Glu-D-Ala)$_2$-]. To ensure accuracy of the models, they were used to calculate structure factors. Indeed, the calculated patterns compared very well with the observed electron diffraction patterns and intensities, thus strongly supporting the efficacy of the proposed models. In the case of c-[(Gln-D-Ala)$_4$-], the diffraction pattern at first appears to give a unit cell one-half the size of that of our model—4.8 Å as opposed to 9.6 Å. However, when diffraction patterns are calculated, every other level of h cancels out due to the pseudo-symmetry of the dimer. That is, the ring flipped over is nearly equivalent to the unflipped ring. Cells where the local two-fold of the dimer is crystalligraphic were also considered, but then the lattice could either not be modeled or the diffraction pattern had to have a mirror plane which was not observed. One other possibility is to consider that the observed diffraction pattern shows a diagonal of the lattice instead of a principle axis. This can be easily dismissed since it requires a substantially smaller unit cell. Therefore, the observed electron diffraction pattern must be due to the principle axis. It should be noted that the overall structural motif of self-assembled nanotube structures has been unequivocally supported in two related but simpler systems by high-resolution single-crystal X-ray crystallography which are in close agreement with the structural assignments made in the present study.

In summary, four new peptide nanotube solid-state ensembles have been described and characterized. These novel biomaterials display remarkable stability under a wide variety of conditions which undoubtedly enhances their utility in a number of future applications. The rationale and design principles detailed in this account are expected to find general application in the design of this and related families of peptide-based biomaterials.

Experimental Section

Chemicals. Acetonitrile (optima grade), dichloromethane (optima grade), dimethylformamide (sequencing grade), and diisopropylamine (peptide synthesis grade) were purchased from Fisher. Dichloromethane and dimethylformamide were dried over 4 Å molecular sieves and stored under nitrogen, diisopropyl amine was either used from a newly opened bottle and used as provided or distilled prior to use. Piperidine was purchased from Aldrich and distilled before use. The following chemicals were used as provided: acetonitrile, trifluoroacetic acid (New

Jersey Halo Carbon), 2-(1H-benzotriazol-1-yl)-1,1,3,3-tetramethyluronium hexafluorophosphate hexafluorophosphate (HBTU), and ((benzotriazol-1-yl)oxy)tris(dimethylamino)phosphonium hexafluorophosphate (BOP) (Richelieau Biotechnologies), amylamine (Sigma), and trifluoroacetic acid-*d* (Isotech). All amino acids were purchased from Bachem California. MBHA resin was purchased from Penninsula Laboratories.

Spectroscopy. One-dimensional ^{1}H NMR spectra were collected on a Bruker AM-300 spectrometer. FT-IR were collected on a Nicolet 550 spectrometer and were deconvoluted using a single-component, mixed Lorentzian and Gaussian function using an iterative, linear least-squares algorithm (FIT, Galactic Industries). Electrospray mass spectrometry (ES-MS) data were collected on a Sciex API 3 mass analyzer. Phase-contrast light microscopy was performed on a Nikon LABOPHOT-2A, and images were taken with a Pentax K1000 at a magnification of 160.

Cryoelectron Microscopy. Cryoelectron microscopy was done according to the procedure previously reported.[10] Nanotubes were absorbed for 1 min on a carbon-coated holey film that had been glow discharged in an atmosphere of amylamine. Excess solution was blotted off with filter paper, and the grid was then quickly immersed in a liquid ethane slush. The grid was then transferred to liquid nitrogen for storage until viewed. The grids were then transferred to a Gatan cryotransfer system at −180 °C and viewed using a Phillips CM12 electron microscope operating a 100 kV. Low-dose conditions were used to photograph nanotube images at high magnifications with a defocus level of 1.5 μm. Samples of c-[(Gln-D-Leu)$_4$-] were imaged with a Philips CM200-T equipped with a Schottky field emission electron source at 200 kV and 1.0 μm defocus. Nanotube electron diffraction patterns were collected at a distance of 1.1 m and measurements standardized by the 111, 220, and 311 diffraction rings of cubic ice contained on the same grid.[13] At least 20 separate diffraction patterns from each sample were collected and analyzed to ensure data consistency and accuracy.

Modeling. Several reasonale models of each nanotube were prepared with XFIT[14] within the unit cell provided from the electron diffraction data. Simulated diffraction spectra were calculated from these models and were compared to the actual diffraction data. The models with the best match were subjected to examination for bad contacts using Procheck.[12] Pictures were prepared using Insight II (Biosym).

Peptide Synthesis. Cyclic peptides were synthesized by the procedure of Rovero *et al.*[15] An orthogonally protected amino acid, *N*-BOC-α-Fm-L-Glu, was used as the first amino acid linked through the side chain to the resin in order to allow peptide cyclization on the solid support. When linked to MBHA resin, this amino acid results in a Gln side chain after HF cleavage. Boc solid-phase synthesis protocols of Kent[16] were used except that DMF flow washes were replaced with 3 × 30 s shake washes. After HF cleavage, the peptides were eluted by sequential washing with ether, 5% aqueous acetic acid, and neat TFA. The ether fraction was discarded, the acetic acid fraction was frozen and lyophilized, and the TFA fraction was evaporated down to a thick residue from which the peptide was precipitated by addition of water. In the case of c-[(Gln-D-Ala)$_4$-], the peptide was found in the acetic acid fraction, while for c-[(Gln-D-Val)$_4$-], c-[(Gln-D-Leu)$_4$-], and c-[(Gln-D-Phe)$_4$-], the peptides were found in the TFA fraction. Peptides were purified by dissolving in neat TFA (c-[(Gln-D-Ala)$_4$-] required 12 h to be completely dissolved), centrifuging at 15000*g* to remove any insoluble impurities, and precipitating the supernatant by addition of 3 volumes of ddH_2O. Suspensions were centrifuged, and the pellet was collected. The procedure was repeated three times to give pure cyclic peptides as judged by ^{1}H NMR and electrospray mass spectrometry.

Self-Assembly and Crystallization. Peptide self-assembly and microcrystal formation was affected by dissolving 10 mg of the peptide in 1 mL of neat TFA and placing it in an open 2 mL Eppendorf tube. The Eppendorf was then floated in a 45 mL conical tube which was filled with 30 mL of ddH_2O. The two solutions were allowed to equilibrate via the gas phase for 48−72 h, after which the Eppendorf was removed and found to have a thick suspension of microcrystals. Crystals were harvested by centrifugation and washed repeatedly with ddH_2O or dialyzed against ddH_2O to remove any remaining TFA. Crystallization yield was quantitative. Stability of nanotubes to highly alkaline solutions as well as FT-IR spectroscopy indicated that TFA did not participate in crystal lattice formation.

Cyclo-[(Gln-D-Ala)$_4$-]. ^{1}H NMR (CF_3COOD, 300 MHz): δ 1.41 (d, J_{HH} = 7.0 Hz, 3H) 2.07 (m, 1H), 2.23 (m, 1H), 2.56 (m, 2H), 4.72 (m, 2H). Positive ES-MS: [M + H] = 797. IR: amide Ia, 1630 cm^{-1}; amide Ib, 1672 cm^{-1}; amide II, 1549 cm^{-1}; N−H stretch, 3282 cm^{-1}.

Cyclo-[(Gln-D-Val)$_4$-]. ^{1}H NMR (CF_3COOD, 300 MHz): δ 0.89 (d, J_{HH} = 6.7 Hz, 3 H), 0.95 (d, J_{HH} = 6.7 Hz, 3H), 2.10 (m, 2H), 2.29 (m, 1H), 2.63 (m, 2H), 4.68 (d, J_{HH} = 6.2 Hz, 1H), 4.82 (dd, J_{HH} = 4.2, 9.4 Hz, 1H). Positive ES-MS: [M + H] = 910. IR: amide Ia, 1630 cm^{-1}; amide Ib, 1687 cm^{-1}; amide II, 1542 cm^{-1}; N−H stretch, 3292 cm^{-1}.

Cyclo-[(Gln-D-Leu)$_4$-]. ^{1}H NMR (CF_3COOD, 300 MHz): δ 0.88 (d, J_{HH} = 4.9 Hz, 3H), 0.89 (d, J_{HH} = 5.1 Hz, 3H), 1.52 (m, 1H), 1.54 (m, 1H), 1.66 (m, 1H), 2.10 (m, 1H), 2.22 (m, 1H), 2.50 (m, 1H), 2.58 (m, 1H), 4.75 (dd, J_{HH} = 11.7, 3.9 Hz, 1H), 4.85 (dd J_{HH} = 4.0, 10.4 Hz, 1H). Positive ES-MS: [M + H] = 965. IR: amide Ia, 1629 cm^{-1}; amide Ib, 1688 cm^{-1}; amide II, 1540 cm^{-1}; N−H stretch, 3278 cm^{-1}.

Cyclo-[(Gln-D-Phe)$_4$-]. ^{1}H NMR (CF_3COOD, 300 MHz): δ 1.59 (m, 1H), 1.74 (m, 1H), 1.88 (m, 2H), 2.88 (dd, J_{HH} = 9.2, 13.6 Hz, 1H), 3.05 (dd, J_{HH} = 6.9, 13.7 Hz, 1H), 4.58 (dd, J_{HH} = 4.8, 8.3 Hz, 1H), 5.08 (dd, J_{HH} = 8.0, 8.0 Hz, 1H), 7.15 (m, 5H). IR: amide Ia, 1629 cm^{-1}; amide Ib, 1678 cm^{-1}; amide II, 1541 cm^{-1}; N−H stretch, 3280 cm^{-1}.

Acknowledgment. We thank colleagues D. McRee for assistance in molecular modeling and M. Sailor for FT-IR spectroscopy. We are grateful to the National Institutes of Health for financial support of this study (GM 52190). M.R.G. is an Alfred P. Sloan Research Fellow (1993−1995) and an Eli Lilly Grantee (1994−1996).

JA953070S

(13) Dubochet, J.; Adrian, M.; Chang, J.-J.; Homo, J.-C.; LePault, J.; McDowall, A. W.; Schultz, P. *Q. Rev. Biophys.* **1988**, *21*, 129−228.

(14) McRee, D. E. *J. Mol. Graphics* **1992**, *10*, 44−46.

(15) Rovero, P.; Quartara, L.; Fabbri, G. *Tetrahedron Lett.* **1991**, *32*, 2639−2642.

(16) Schnolzer, M.; Alewood, P.; Jones, A.; Alewood, D.; Kent, S. B. H. *Int. J. Pept. Protein Res.* **1992**, *40*, 180−193.